Knocking out USP7 attenuates cardiac fibrosis and endothelial-to-mesenchymal transition by destabilizing SMAD3 in mice with heart failure with preserved ejection fraction

Shuai Yuan[1]*; Zimu Wang[1]*; Shun Yao[1]*; Yanyan Wang[1]*; Zhonglei Xie[1]; Jingfeng Wang[1]; Xueting Yu[1]; Yu Song[1]; Xiaotong Cui[1]; Jingmin Zhou[# 1], Junbo Ge[# 1]

1. Department of Cardiology, Shanghai Institute of Cardiovascular Diseases, Zhongshan Hospital, Fudan University, Shanghai, China.

Short title: Knocking out USP7 Attenuates HFpEF

#Correspondence to: Jingmin Zhou and Junbo Ge, Department of Cardiology, Shanghai Institute of Cardiovascular Diseases, Zhongshan Hospital, Fudan University, 180 Fenglin Road, Xuhui District, Shanghai, 200032, China.

E-mail: zhou.jingmin@zs-hospital.sh.cn; jbge@zs-hospital.sh.cn

*: These autors contributed equally to this work.

Abstract

Background: Heart failure with preserved ejection fraction (HFpEF) is a predominant type of heart failure. Exploring new pathogenesis and identifying potential novel therapeutic targets for HFpEF is of paramount importance.

Methods: HFpEF mouse model was established by the "Multiple-hit" strategy, in that 18- to 22-month-old female C57B6/J mice fed with a high-fat diet were further challenged with chronic infusion of Angiotensin II. RNA sequencing analysis showed that USP7 was significantly increased in the heart of HFpEF mice. Liquid chromatography coupled with tandem mass spectrometry (LC-MS/MS) analysis, in conjunction with co-immunoprecipitation (Co-IP) techniques, identified expression of SMAD3, the key molecule of endothelial-to-mesenchymal transition (EndMT), was also significantly elevated. USP7 endothelium-specific knockout mice was generated to investigate the involvement of USP7 in HFpEF. The biological significance of the interaction between USP7 and SMAD3 was further explored.

Results: USP7 promotes EndMT and cardiac fibrosis by binding to SMAD3 directly via its UBL (Ubiquitin-like) domain and cysteine at position 223 of USP7, leading SMAD3 deubiquitination to maintain the stability of SMAD3 by removing the K63 ubiquitin chain and preventing the degradation of SMAD3 by proteasomal process. USP7 also promotes SMAD3 phosphorylation and nuclear translocation, thereby aggravating EndMT and cardiac fibrosis. Endothelium-specific USP7 knockout led to improvement of HFpEF phenotypes and reduction of cardiac fibrosis. Overexpression of SMAD3 in endothelium-specific knockout HFpEF mice reversed the protective effects of USP7 knockout in this HFpEF mouse model.

Conclusion: Our results indicated that USP7 is one of the key pathogenic molecules of HFpEF, and

40   knocking out USP7 could attenuate HFpEF injury by promoting the degradation of SMAD3. USP7

41   and SMAD3 inhibition might be potential therapeutic options for HFpEF.

42   **Key words:** USP7; Deubiquitination enzyme; Heart failure with preserved ejection fraction;

43   Endothelial-to-mesenchymal transition; Cardiac fibrosis.

44

45   **Graphical Abstract**

46
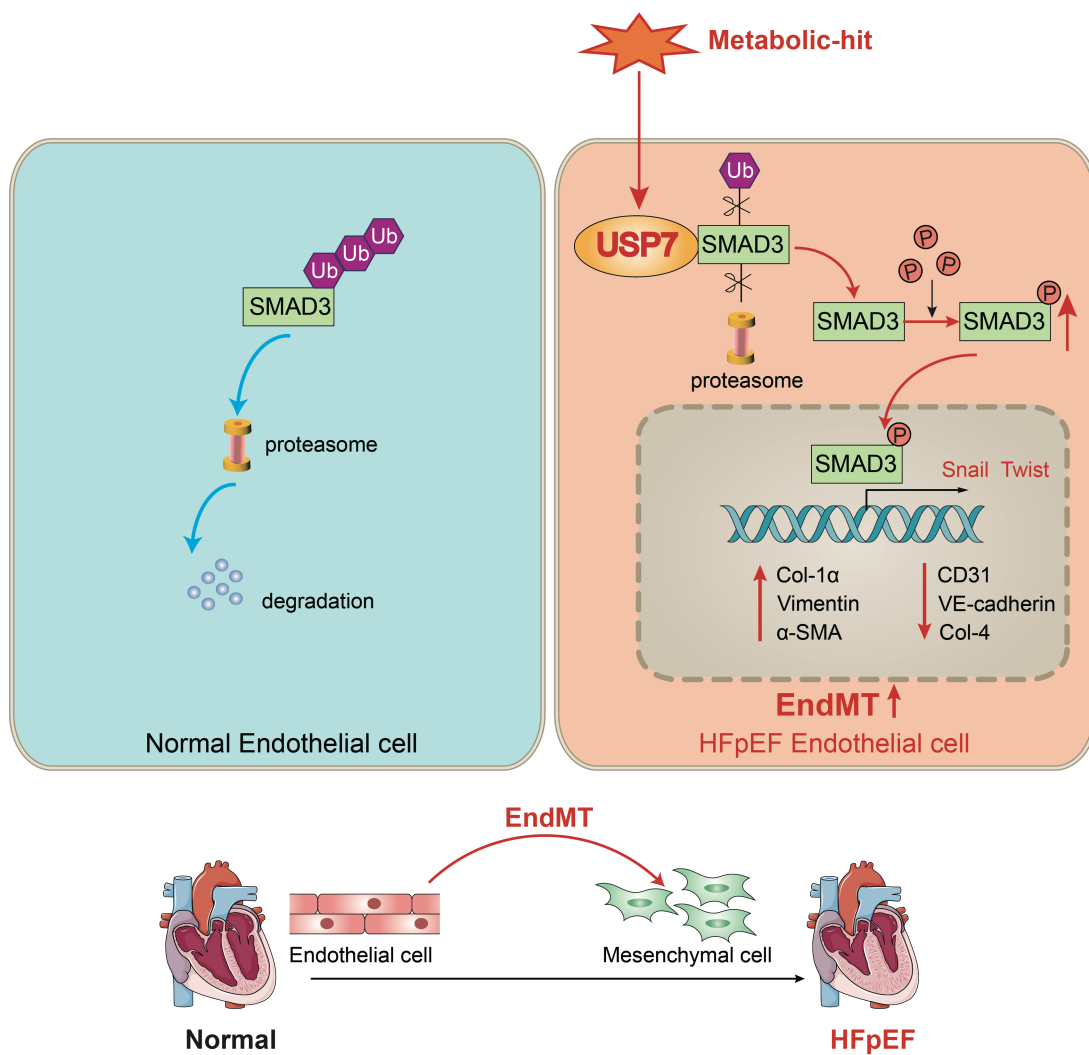
Introduction

Heart failure (HF) is a clinical syndrome causing significant morbidity, mortality, and healthcare expenditure. Heart failure with preserved ejection fraction (HFpEF) is a predominant type of heart failure, representing approximately 50% of all HF cases[1]. Given the aging population and the ongoing epidemics of metabolic disorders and hypertension, the prevalence of HFpEF is expected to rising continuously in the future[2, 3]. However, HFpEF has shown poor response to the standard treatment approach used for heart failure with reduced ejection fraction (HFrEF). Major clinical trials conducted have not yielded positive results on primary outcomes until the era of angiotensin receptor–neprilysin inhibitor (ARNI) sacubitril/valsartan and the sodium–glucose cotransporter 2 inhibitor (SGLT2i) empagliflozin[4-6]. Exploring the pathogenesis and identifying potential therapeutic targets for HFpEF is thus of paramount importance to develop novel therapeutic targets.

There is growing recognition that cardiac fibrosis plays a significant role in the etiology of all types of HF, particularly in the pathophysiology of HFpEF[7, 8]. Among the multiple factors contributing to the development of HFpEF, fibrosis serves as a major pathogenic factor irrespective of the underlying etiology. It has been observed that the extracellular fibrotic burden exhibits a stronger correlation with diastolic dysfunction and is also associated with increased hospitalization and mortality in HFpEF[9, 10]. Options to attenuate fibrosis thus draw significant attention on alleviating HFpEF phenotypes. However, in contrast to cardiac fibrosis observed in HFrEF, characterized by the replacement of cardiomyocyte loss with extracellular matrix (ECM) proteins to preserve the structural integrity of the myocardium, cardiac fibrosis in HFpEF is considered to be reactive fibrosis occurring in the context of systemic inflammation and metabolic abnormalities in the setting of non-significant cardiomyocyte death[11]. In this reactive fibrosis process, a series

69 of reactions resulted from endothelial inflammation, such as impaired nitric oxide (NO) utilization,

70 and increased adhesion of inflammatory cells, which serve as significant driving factors for

71 enhanced fibrosis and ventricular remodeling in HFpEF[12]. Under conditions of systemic

72 inflammation, dysfunctional endothelial cells (ECs) have been observed to undergo a phenotypic

73 transformation into a mesenchymal-like state, commonly referred to as endothelial-mesenchymal

74 transition (EndMT)[13, 14]. Previous studies have demonstrated that EndMT could contribute to

75 the process of cardiac fibrosis[15-17]. While myofibroblasts are traditionally recognized as the

76 primary contributors to fibrosis, there is an increasing recognition of the crucial role played by

77 EndMT in myocardial fibrosis. It is known that EndMT may function as an intermediate process

78 linking endothelial inflammation and ventricular remodeling in HFpEF[18]. Thus, targeting EndMT

79 might emerge as a novel therapeutic strategy for managing HFpEF.

80 Ubiquitination, as a crucial posttranslational modification, plays a significant role in various cellular

81 processes including cell signal transduction, cell fate determination, inflammatory responses, and

82 other essential biological activities[19, 20]. Ubiquitination is a reversible process that can be

83 counter-regulated by deubiquitinating enzymes (DUBs). DUBs are essential for maintaining cellular

84 signaling networks and are involved in various aspects of pathophysiology by precisely controlling

85 protein function, localization, and degradation. Approximately 100 deubiquitinating enzymes

86 (DUBs) have been identified, and they play a significant role in regulating intracellular signal

87 transduction. These DUBs have been found to be closely associated with various cardiovascular

88 diseases[21-23]. However, the exact involvement of DUBs in the pathogenesis of HFpEF is not

89 fully understood.

90 In our experiment, we examined the expression of DUBs in HFpEF mice induced by a combined

91   set of risk factors, including age, obesity, and hypertension, referred to as the "Multiple-hit"

92   Strategy[24]. We identified significantly upregulated level of a DUB, USP7(ubiquitin-specific

93   protease 7), also known as herpes virus-associated ubiquitin-specific protease (HAUSP), in heart

94   tissues of HFpEF mice. Furthermore, our findings revealed that the observed increase in USP7

95   expression was predominantly localized within endothelial cells in HFpEF mice. To examine the

96   specific role of USP7 in endothelial cells, we generated endothelial cell-specific USP7 knockout

97   mice. Our results provided evidence that the deficiency of USP7 in endothelial cells improved

98   diastolic dysfunction, reduced BNP, fibrosis and EndMT in HFpEF model. Detailed mechanistic

99   studies showed that USP7 deficiency blocked its interaction with SMAD3, leading to enhanced

100   degradation and inactivation of SMAD3. SMAD3 overexpression reversed the protective effects of

101   USP7 deficiency in this HFpEF model. Our results thus hint that targeting USP and/or SMAD3

102   might serve as promising therapeutic options for the treatment of HFpEF.

103

104   ## Methods

105   All data, methods, and study materials will be made available to other researchers for the purposes

106   of reproducing our results or replicating the procedures. Detailed methods are provided in the

107   Supplemental Material.

108   **Animal Studies**

109   WT mice (C57BL/6J) were purchased from Beijing Vital River Laboratory Animal Technology Co.,

110   Ltd (Beijing, China). $USP7^{flox/flox}$ mice and Cdh5-Cre^{ERT} mice on C57BL/6J background, aged 8-10

111   months, were purchased from Cyagen (Suzhou, China). Endothelial-specific conditional USP7

112   deficiency mice ($USP7^{flox/flox}$/Cdh5-Cre^{ERT}) were generated by crossing $USP7^{flox/flox}$ mice with

113   Cdh5-Cre^{ERT} mice and intraperitoneally injected with tamoxifen (30 mg/kg) daily for 5 days. All

114   animal experiments complied with the Guide for the Care and Use of Laboratory Animals published

115   by the US National Institutes of Health (publication No. 85-23, revised 1996) and permitted by the

116   Animal Care and Use Committee of Zhongshan Hospital, Fudan University.

117   **Statistical Analysis**

118   Data were reported as Mean ± SEM. For n ≥ 6 data, the Shapiro-Wilk normality test was conducted

119   to assess the normality of the data. Fisher's exact test was utilized to compare categorical variables.

120   For data with a normal distribution, the unmatched two-tailed Student's t-test was employed to

121   determine whether the difference between the two groups was statistically significant. For multi-

122   group comparison, one-way or two-way ANOVA with Tukey's multiple comparison test or Šidák

123   test was utilized. For datasets with n < 6 or non-normal distribution, the non-parametric unpaired

124   Mann-Whitney test was used to assess the statistical significance of the difference between the two

125   groups. A statistically significant difference was obtained at $P < 0.05$. Data were analyzed by

126   GraphPad Prism software (version 9.4.1, CA, USA) and R (Version 4.2.3).

127

128   # Results

129   **Endothelial USP7 expression is upregulated in HFpEF mice generated by the Mutiple-hit**

130   **strategy**

131   To establish the HFpEF phenotypes, female mice (18 - 22 months old) were fed a high-fat diet for

132   12 weeks and infused with angiotensin II (Ang II) at a dosage of 1.25 mg/kg/day from the 8th week

133   to the 12th week (**Figure 1A**). These HFpEF mice recapitulate human HFpEF by demonstrating

134   hypertension, obesity, exercise intolerance, lung congestion, left ventricular (LV) hypertrophy, and

hemodynamic evidence of diastolic dysfunction, featured by higher E/e', while LV ejection fraction

(EF) remains preserved (**Figure S1-2**). Histopathologic data showed that hearts of HFpEF mice

exhibited cardiac hypertrophy, pronounced collagen deposition, microvascular rarefaction and

interstitial fibrosis (**Figure S3**). Recent years have witnessed an increasing body of evidence

implicating DUBs in the pathogenesis of heart failure. Through transcriptome sequencing, we

observed significantly differentiated expression of a large number of DUBs in the myocardial tissue

of HFpEF mice (**Figure 1B, Figure S5, Table S1**). Additionally, mRNA expression of the DUBs

was detected through transcriptome sequencing and results showed that the transcription of USP7

was significantly upregulated in HFpEF mice (**Figure 1B-C**). Immunofluorescence staining on the

extracted cells from the hearts of HFpEF mice and subsequent western blotting experiments showed

that the upregulation of USP7 was primarily localized in the endothelial cells (**Figure 1D through**

1G, Figure S4). Collectively, these results indicated the upregulation of endothelial USP7 in this

HFpEF model.

Endothelium-specific knockout of USP7 alleviates cardiac fibrosis by mitigating EndMT,

thereby ameliorating the HFpEF phenotypes

USP7 knockout led to early embryonic lethality[25]. Endothelial-specific conditional USP7

deficiency mouse (*USP7*^{flox/flox}/Cdh5-Cre^{ERT}; USP7-ECKO) were generated by crossing *USP7*^{flox/flox}

mice with Cdh5-Cre^{ERT} mice and intraperitoneally injected with tamoxifen (30 mg/kg) daily for 5

days (**Figure S6**). To examine the functional significance of endothelial USP7 activation in HFpEF

mice, *USP7*^{flox/flox} and USP7-ECKO mice were stimulated with the "Multiple-hit" strategy. After

"Multiple-hit" strategy, USP7-ECKO mice exhibited a lower heart weight-to-tibia length ratio

157 (HW/TL), lower lung weight wet/dry ratio, and improved exercise tolerance compared to

158 *USP7*flox/flox mice (**Figure 2A and 2B, Figure S7B**). However, no significant difference in body

159 weight and blood pressure were observed between 2 groups (**Figure S7A**). Serum BNP levels and

160 TGFβ1 levels were found to be decreased in USP7-ECKO mice compared to *USP7*flox/flox HFpEF

161 mice (**Figure 2F, Figure S7J**). Echocardiography results demonstrated partial improvement in

162 diastolic function in mice with USP7-ECKO mice, as reflected by E/e', -GLS and IVRT as

163 compared to *USP7*flox/flox HFpEF mice (**Figure 2C through 2E, Figure S7E**). Tissue section

164 staining revealed that cardiac fibrosis and microvascular rarefaction were ameliorated, and EndMT

165 was alleviated in mice with EC-specific knockout of USP7 (**Figure 2J through 2L, Figure S8**).

166 Western blot assay and RT-qPCR further demonstrated that the EC-specific knockout of USP7 could

167 alleviate the reduction in endothelial phenotype expression and the increase in interstitial phenotype

168 expression induced by the "Multiple-hit" strategy (**Figure 2M and 2N, Figure S7K**).

169

170 **USP7 is involved in endothelial EndMT in vitro**

171 Based on the increased expression of USP7 in endothelial cells of HFpEF mice and the observed

172 partial improvement in cardiac fibrosis and EndMT following EC-specific knockout of USP7 in this

173 in vivo HFpEF model, we hypothesized that USP7 might alleviate HFpEF cardiac fibrosis by

174 regulating the EndMT process in the setting of HFpEF. To prove this concept, we isolated primary

175 cardiac microvascular endothelial cells (CMECs) from lactating rats. Results showed that USP7

176 expression was upregulated in the process of EndMT upon TGFβ1 stimulation in a time-dependent

177 manner and the most significant increase in USP7 expression upon TGFβ1 stimulation was found

178 at the concentration of 10 ng/ml, consistent with the observations in the animal model (**Figure 3A**

179   **Through 3D**). Additionally, reducing the protein expression of USP7 through short hairpin RNA

180   lentiviral particles targeting USP7 (shUSP7) transfection resulted in the amelioration of EndMT

181   under TGFβ1 stimulation, characterized by an increase in the endothelial cell phenotype and a

182   decrease in the interstitial phenotype (**Figure 3E through 3K, Figure S10**). These findings suggest

183   that USP7 plays a crucial role in the regulation of EndMT in cardiac endothelial cells.

184

185   **USP7 directly interacts with SMAD3, with SMAD3 being one of the crucial substrates of USP7**

186   It is known that DUBs could modulate biological activities by influencing the degradation or

187   function of substrate proteins[26]. In order to identify the substrate proteins involved in EndMT and

188   regulated by USP7, we extracted the proteins of cardiac tissue from HFpEF mice and conducted a

189   screening of potential substrate proteins using co-immunoprecipitation (Co-IP) in conjunction with

190   Liquid chromatography coupled with tandem mass spectrometry (LC-MS/MS) analysis. After

191   excluding the peptides related to the light and heavy chains of the antibody, SMAD3, a key molecule

192   involved in the regulation of EndMT, was found to be a potential substrate for USP7 (**Figure 4A**

193   **and 4B**). As shown in **Figure 4C and 4D**, knockdown of USP7 expression resulted in a reduction

194   in the expression of SMAD3, indicating a regulatory relationship in that USP7 could influence

195   SMAD3 expression. However, the reverse scenario, where knocking down the expression of

196   SMAD3 does not have a significant impact on USP7 expression, suggests that SMAD3 is the

197   downstream signaling of USP7 (**Figure 4E and 4F**). Furthermore, TGFβ1 stimulation further

198   enhanced the interaction between USP7 and SMAD3 in CMECs (**Figure 4G and 4H**). Subsequently,

199   USP7 and SMAD3 plasmids were co-transfected into 293T cells and their interaction was confirmed

200   by visualizing the co-localization of USP7 and SMAD3 (**Figure 4I and 4J**). USP7 consists of 3

domains: a TRAF (TNF receptor-associated factor) domain, a CAT (Cysteine-rich domain

Associated with TRAF1) domain, and a UBL (Ubiquitin-like) domain[27]. To further elucidate the

specific domain of USP7 that interacts with SMAD3, three USP7 mutants were generated. Results

of co-transfection of SMAD3 and the respective mutated USP7 plasmids in 293T cells showed that

the USP7 mutant containing amino acids 561-1102 retained the ability to bind to SMAD3, while

mutants in other domains failed to interact with SMAD3 (**Figure 4K and 4L**). Above findings

demonstrate that USP7 directly binds to SMAD3, and this interaction is mediated by the UBL

domain of USP7. Similarly, we constructed 3 mutant plasmids of SMAD3 (MH1, Linker and MH2

domain) and found that SMAD3 interacted with USP7 through MH2 domain (**Figure S13**).

USP7 regulates the stability of SMAD3 protein through deubiquitination process

The interaction and regulatory relationship between USP7 and SMAD3 raise the question of how

USP7 regulates SMAD3. Interestingly, we observed a decrease in SMAD3 protein levels upon

reducing USP7 expression, and this decrease was not attributed to altered transcription of SMAD3

(**Figure 5A and 5B**). This suggests that USP7 may regulate SMAD3 at the post-translational level,

possibly through protein stabilization or degradation pathways. We hypothesized that USP7 might

prevent the intracellular degradation of SMAD3. In fact, cycloheximide (CHX) pulse-chase assay

revealed that USP7 obviously prevented SMAD3 from proteasomal degradation (**Figure 5C and**

5D). This indicated that USP7 might play a role in mitigating degradation of SMAD3 protein. It is

known that USP7 might function as a deubiquitylating enzyme, exert its regulatory role by removing

ubiquitin molecules from target proteins. The exact regulatory mechanism of USP7 in SMAD3

ubiquitination was explored. Myc-SMAD3 and ubiquitin plasmids were co-transfected into 293T

223 cells. Subsequently, the transfected cells were divided into two groups: one group was transfected

224 with Flag-USP7 plasmid, while the other group was transfected with Flag-vector plasmid as a

225 control. Then, the cells were treated with MG132 to inhibit proteasomal degradation of the SMAD3

226 protein. Notably, a significant decrease was observed in the presence of ubiquitin molecules on

227 SMAD3 in cells transfected with the Flag-USP7 plasmid compared to cells transfected with the

228 Flag-vector plasmid (**Figure 5E**). It has been reported that cysteine at position 223 was crucial for

229 USP7 to exert its deubiquitination function[27]. To further identify the deubiquitination sites of

230 USP7, a catalytic mutant USP7 (C223S) was constructed. Results showed that the catalytic mutant

231 USP7 (C223S) failed to reduce the ubiquitination level of SMAD3, and could not affect the binding

232 of them (**Figure 5F and 5G**). To investigate the specific ubiquitin chains recognized by USP7, we

233 further generated ubiquitin plasmids retain only K48 or K63 active sites. Results showed that USP7

234 primarily exerts its deubiquitination function by recognizing and cleaving ubiquitin chains at the

235 K63 sites (**Figure 5H**). These results thus indicate that USP7 could remove K63-linked ubiquitin

236 molecules from SMAD3 and prevent SMAD3 from proteasomal degradation, and the cysteine at

237 position 223 of USP7 is implicated in the removal of ubiquitin molecules from SMAD3, thereby

238 preventing its degradation.

239

240 **USP7 regulates EndMT by stabilizing SMAD3 and accumulating phosphorylated SMAD3**

241 To further define the mechanistic role of SMAD3 in the USP7-mediated EndMT process, effects of

242 overexpressing SMAD3 while simultaneously knocking down USP7 were observed in CMECs. The

243 results indicated that the improvement in the EndMT phenotype resulting from the knockdown of

244 USP7 was partially attenuated by overexpressing SMAD3 (**Figure 6A, Figure S14**). The process

245 of SMAD3 activation contains phosphorylation and nuclear translocation. We demonstrated that

246 down-regulation of USP7 reduced the protein level of SMAD3 in the previous part. However,

247 whether this down-regulation could indirectly lead to the decrease of phosphorylated SMAD

248 remains unclear. Therefore, we then explored whether USP7 could modulate the levels of

249 phosphorylated SMAD3 (p-SMAD3). Results showed that knocking down USP7 resulted in a

250 reduction of the elevated levels of pSMAD3 induced by TGFβ1 (**Figure 6B**). Interestingly, further

251 nuclear-cytoplasmic separation assays and immunofluorescence staining experiments provided

252 additional evidence in that knocking down USP7 impeded the translocation of pSMAD3 into the

253 nucleus (**Figure 6C and 6D**). These in vitro study results thus demonstrate that USP7 could regulate

254 the phosphorylation and nuclear translocation of SMAD3, ultimately modulate the EndMT process

255 in CMECs stimulated by TGFβ1.

256

257 **USP7 knocking out ameliorates cardiac fibrosis and EndMT of HFpEF via SMAD3-dependent**

258 **pathway in vivo**

259 To validate the role of SMAD3 in USP7 knocking out-mediated beneficial effects in this HFpEF

260 model, we constructed AAV9-ENT vectors (based on adeno-associated virus 9 (AAV9) serotype

261 modification and enhanced the infection efficiency of vascular endothelial cells) carrying SMAD3

262 under the ICAM2 promoter. And then delivered these AAV9-ENT vectors via cardiac injection in

263 situ (**Figure 7A**). We confirmed that SMAD3 was highly expressed in cardiac ECs of HFpEF mice

264 (**Figure S15**). Injection of AAV9-ENT did not have a significant effect on weight gain and blood

265 pressure following the "Multiple-hit" strategy in mice (**Figure S16**). The heart weight-to-tibial

266 length ratio (HW/TL), lung weight/dry ratio, and exercise tolerance measurements indicated that

267 myocardial overexpression of SMAD3 in EC-specific USP7 knockout mice reversed the protected

268 effects of knocking out USP7 in the HFpEF phenotypes induced by the "Multiple-hit" strategy

269 (**Figure 7B and 7C**). Additionally, it was observed that myocardial overexpression of SMAD3 in

270 EC-specific USP7 knockout mice reversed the protective effects of EC-specific USP7 knockout in

271 terms of cardiac function, fibrosis, and EndMT post the "Multiple-hit" strategy (**Figure 7D through**

272 **7F, Figure S16**). Serum BNP levels changed in line with above changes (**Figure 7G**).

273

Discussion

275 Our study revealed that USP7 plays a pivotal role in the progression of cardiac fibrosis in HFpEF

276 mice by promoting the process of EndMT. The novel findings of our study are as follows: 1.

277 upregulation of USP7 and SMAD3 was identified in the cardiac microvascular endothelial cells of

278 the "Multiple-hit" HFpEF mouse model; 2. EC-specific knockout of USP7 significantly ameliorated

279 cardiac diastolic dysfunction, reduced cardiac fibrosis, and mitigated EndMT in HFpEF mice; 3.

280 Mechanistically, USP7 could remove K63-linked ubiquitin molecules from SMAD3 and prevent

281 SMAD3 from proteasomal degradation, and the cysteine at position 223 of USP7 was implicated in

282 the removal of ubiquitin molecules from SMAD3, thereby preventing its degradation, USP7 thus

283 enhanced the stability of SMAD3 and regulated the phosphorylation and nuclear translocation of

284 SMAD3, thereby facilitating the transcription of genes related to EndMT. Collectively, our study

285 demonstrated knocking out USP7 could ameliorate diastolic dysfunction and reduce cardiac fibrosis

286 through promoting the degradation of SMAD3 in HFpEF, primarily by mitigating the process of

287 EndMT (**Figure 8**). Inhibiting USP7 and SMAD3 might be feasible ways to alleviate HFpEF

288 pathology.

289   The development of effective, evidence-based treatments for HFpEF is challenged by the

290   phenotypic heterogeneity and the complexity of underlying pathogenesis of HFpEF[28, 29]. One

291   important obstacle is the absence of the animal model that accurately replicates the complexities of

292   human HFpEF[30, 31]. Patients with HFpEF usually present with multiple comorbidities, including

293   obesity, hypertension, diabetes, and other metabolic disorders[3, 32]. Several research groups

294   developed animal models for HFpEF, each of them with distinctive strengths and limitations. The

295   efficacy of animal models could be partially evaluated in the two recent HFpEF scoring systems[33,

296   34]. In our study, the animal model got a score of 4 points in the H2PEF scoring system and 5 points

297   in the HFA-PEF scoring system, which was consistent with the results of previous study[24]. This

298   suggests that the HFpEF model used in this study resembles the human clinical situation to some

299   extent.

300   EndMT is the process in which endothelial cells (ECs) transform into mesenchymal cells. This

301   phenomenon is implicated in a variety of cardiovascular diseases, including valve disease,

302   myocardial infarction (MI), fibrosis, endocardial fibroelastic fibrosis, atherosclerosis, and

303   pulmonary arterial hypertension (PAH)[14]. A recent study demonstrated that in vitro cultivation of

304   human aortic endothelial cells using serum obtained from patients with HFpEF could stimulate

305   endothelial EndMT and there is thus a close clinical association between EndMT and HFpEF[35].

306   In line with this finding, our results hinted that alleviated HFpEF phenotypes was related to reduced

307   EndMT in our HFpEF model post USP7 knocking out.

308   DUBs can modify the signal transmission and protect substrate proteins from degradation by

309   regulating the form of ubiquitin molecule linkage. Understanding the regulatory mechanisms of

310   DUBs in HFpEF is anticipated to yield novel therapeutic strategies. Previous studies have also

311 demonstrated that DUBs are implicated in a range of cardiovascular diseases, including cardiac

312 hypertrophy[36, 37], cardiomyopathy[38], and vascular remodeling[39]. However, as far as our

313 knowledge extends, there were no prior studies investigating the functioning of DUBs in HFpEF.

314 Our study revealed significant upregulation of USP7 in the cardiac microvascular endothelium of

315 HFpEF mice, and EC-specific knockout of USP7 improved HFpEF phenotypes, including cardiac

316 diastolic function, myocardial fibrosis, and exercise tolerance in HFpEF mice, indicating a crucial

317 role of USP7 in the pathogenesis of HFpEF.

318 The role of DUBs is closely related to the function of the substrate proteins. Through LC-MS/MS,

319 we identified SMAD3 as a substrate of USP7. This finding was further confirmed through co-

320 immunoprecipitation (Co-IP) experiments. The TGFβ-SMAD3 signaling pathway serves as a

321 primary inducer of EndMT, SMAD3 is activated through phosphorylation, subsequently

322 translocating into the nucleus to regulate the transcription of proteins associated with EndMT[40].

323 Previous studies demonstrated that the specific knockdown or inhibition of SMAD3 could

324 effectively mitigate EndMT[41, 42]. Ubiquitination is one of the key mechanisms involved in the

325 degradation of SMAD3[43]. Simultaneously, DUBs possess the capability to inhibit the

326 ubiquitination and subsequent degradation of SMAD3, enabling precise regulation of SMAD3

327 levels. OTUB1, UCHL5, OTUD1 and USP15 have been reported to participate in the regulation of

328 SMAD3 deubiquitination, and the abnormal expression of DUBs disrupts the dynamic balance of

329 SMAD3, consequently promoting the development of various pathological processes[39, 44-46]. It

330 had been reported that USP7 could influence the progression of p53-negative lung cancer by

331 regulating SMAD3[47]. In our study, we demonstrated that the abnormal activation of USP7 might

332 not lead to beneficial effects in HFpEF. Due to the abnormal activation of USP7, SMAD3 was

15

333   upregulated, which in turn increased the EndMT process of ECs, promoted myocardial fibrosis, and

334   accelerated the progression of HFpEF. Inhibiting the abnormal activation of USP7 in ECs might be

335   an effective target to improve the prognosis of HFpEF. This suggested that USP7 might play

336   different roles in different diseases and cell types. Our study complemented the existing research by

337   addressing the role of USP7 in the field of HFpEF. In addition, our study also showed that during

338   EndMT in CMECs, USP7 primarily influenced the post-translational modification process. USP7

339   removed K63-linked ubiquitin molecules from SMAD3, preventing its proteasomal degradation.

340   Our research enriched the understanding of regulatory mechanism between USP7 and SMAD3.

341   Briefly, we identified USP7 as a crucial DUB that regulates SMAD3 and play pivotal role in the

342   EndMT process of HFpEF cardiac fibrosis. Our results showed that USP7 sustained SMAD3

343   stability via promoting deubiquitination of SMAD3, reversing K63-linked ubiquitin chains in the

344   cysteine at position 223 of USP7. Furthermore, USP7 also enhanced the activation of SMAD3 by

345   promoting SMAD3 phosphorylation. Identifying the specific active site of USP7 that regulates

346   SMAD3 ubiquitination can streamline drug development targeting this specific site, without

347   impacting the functions of substrate proteins at other active sites of USP7, and thereby minimizing

348   potential drug side effects.

349   Some limitations of this study should be acknowledged. First, the improvement in the HFpEF

350   phenotypes achieved through EC-specific knockout of USP7 may not solely be attributed to the

351   regulation of SMAD3 to alleviate EndMT. Other potential mechanisms may also be involved, as

352   evidenced by the reduced plasma TGFβ1 levels observed in mice with EC-specific knockout of

353   USP7 (**Figure S7J**). Second, in vitro experiments may not entirely replicate the conditions under

354   which EndMT occurs in the complex "Multiple-hit" state of the HFpEF phenotypes. Additionally,

there may be other pathways contributing to the process of EndMT in our HFpEF model, such as metabolic transitions. Further investigations are also required to explore if there is an add-on effects on HFpEF by jointly inhibition of USP7 and SMAD3. Third, because of the challenges in acquiring myocardial tissue samples from HFpEF patients, our dataset lacked validation from patient myocardial tissue. Further validation of the HFpEF phenotypes in humans would enhance the clinical translational significance of this study.

In conclusion, our study unveiled the pivotal role of USP7 in endothelial cells as a key regulator of EndMT in the context of HFpEF. EC-specific knockout of USP7 could ameliorate cardiac diastolic function, reduce cardiac fibrosis, and mitigate EndMT in HFpEF mice in a SMAD3 dependent pathway. Our studies hinted that inhibiting USP7 and SMAD3 alone or in combination might be potential therapeutic option for the management of HFpEF.

Acknowledgments

Author Contributions

The study was designed by Jingmin Zhou. and Junbo Ge. The experiments were conducted by Shuai Yuan, Zimu Wang, Shun Yao, Yanyan Wang, Zhonglei Xie, Jingfeng Wang, Xueting Yu and Yu Song. The data were analyzed by Shuai Yuan, Zimu Wang and Zhonglei Xie. The article was written by Shuai Yuan, Zimu Wang, Xiaotong Cui, Jingmin Zhou and approved by all authors.

Sources of Funding

Disclosures

None.

Reference

1. Heidenreich PA, Bozkurt B, Aguilar D, Allen LA, Byun JJ, Colvin MM, et al. 2022 AHA/ACC/HFSA Guideline for the Management of Heart Failure: A Report of the American College of Cardiology/American Heart Association Joint Committee on Clinical Practice Guidelines. Circulation. 2022; 145: e895-e1032.

2. Tsao CW, Lyass A, Enserro D, Larson MG, Ho JE, Kizer JR, et al. Temporal Trends in the Incidence of and Mortality Associated With Heart Failure With Preserved and Reduced Ejection Fraction. JACC Heart Fail. 2018; 6: 678-85.

3. Shah SJ, Borlaug BA, Kitzman DW, McCulloch AD, Blaxall BC, Agarwal R, et al. Research Priorities for Heart Failure With Preserved Ejection Fraction: National Heart, Lung, and Blood Institute Working Group Summary. Circulation. 2020; 141: 1001-26.

4. Redfield MM, Borlaug BA. Heart Failure With Preserved Ejection Fraction: A Review. JAMA. 2023; 329: 827-38.

5. Anker SD, Butler J, Filippatos G, Ferreira JP, Bocchi E, Böhm M, et al. Empagliflozin in Heart Failure with a Preserved Ejection Fraction. N Engl J Med. 2021; 385: 1451-61.

6. Mentz RJ, Ward JH, Hernandez AF, Lepage S, Morrow DA, Sarwat S, et al. Angiotensin-Neprilysin Inhibition in Patients With Mildly Reduced or Preserved Ejection Fraction and Worsening Heart Failure. J Am Coll Cardiol. 2023; 82: 1-12.

7. González A, Schelbert EB, Díez J, Butler J. Myocardial Interstitial Fibrosis in Heart Failure: Biological and Translational Perspectives. J Am Coll Cardiol. 2018; 71: 1696-706.

8. Moreo A, Ambrosio G, De Chiara B, Pu M, Tran T, Mauri F, et al. Influence of myocardial fibrosis on left ventricular diastolic function: noninvasive assessment by cardiac magnetic resonance and echo. Circ Cardiovasc Imaging. 2009; 2: 437-43.

9. Zile MR, Baicu CF, Ikonomidis JS, Stroud RE, Nietert PJ, Bradshaw AD, et al. Myocardial stiffness in patients with heart failure and a preserved ejection fraction: contributions of collagen and titin. Circulation. 2015; 131: 1247-59.

10. Kanagala P, Cheng ASH, Singh A, Khan JN, Gulsin GS, Patel P, et al. Relationship Between Focal and Diffuse Fibrosis Assessed by CMR and Clinical Outcomes in Heart Failure With Preserved Ejection Fraction. JACC Cardiovasc Imaging. 2019; 12: 2291-301.

413   11.   Mishra S, Kass DA. Cellular and molecular pathobiology of heart failure with preserved
414   ejection fraction. Nat Rev Cardiol. 2021; 18: 400-23.

415   12.   Paulus WJ, Tschöpe C. A novel paradigm for heart failure with preserved ejection fraction:
416   comorbidities drive myocardial dysfunction and remodeling through coronary microvascular
417   endothelial inflammation. J Am Coll Cardiol. 2013; 62: 263-71.

418   13.   Bischoff J. Endothelial-to-Mesenchymal Transition. Circ Res. 2019; 124: 1163-5.

419   14.   Li Y, Lui KO, Zhou B. Reassessing endothelial-to-mesenchymal transition in cardiovascular
420   diseases. Nat Rev Cardiol. 2018; 15: 445-56.

421   15.   Widyantoro B, Emoto N, Nakayama K, Anggrahini DW, Adiarto S, Iwasa N, et al. Endothelial
422   cell-derived endothelin-1 promotes cardiac fibrosis in diabetic hearts through stimulation of
423   endothelial-to-mesenchymal transition. Circulation. 2010; 121: 2407-18.

424   16.   Murdoch CE, Chaubey S, Zeng L, Yu B, Ivetic A, Walker SJ, et al. Endothelial NADPH oxidase-
425   2 promotes interstitial cardiac fibrosis and diastolic dysfunction through proinflammatory effects
426   and endothelial-mesenchymal transition. J Am Coll Cardiol. 2014; 63: 2734-41.

427   17.   Li Z, Xia H, Sharp TE, 3rd, LaPenna KB, Katsouda A, Elrod JW, et al. Hydrogen Sulfide
428   Modulates Endothelial-Mesenchymal Transition in Heart Failure. Circ Res. 2023; 132: 154-66.

429   18.   D'Amario D, Migliaro S, Borovac JA, Restivo A, Vergallo R, Galli M, et al. Microvascular
430   Dysfunction in Heart Failure With Preserved Ejection Fraction. Front Physiol. 2019; 10: 1347.

431   19.   Roberts JZ, Crawford N, Longley DB. The role of Ubiquitination in Apoptosis and Necroptosis.
432   Cell Death Differ. 2022; 29: 272-84.

433   20.   Cockram PE, Kist M, Prakash S, Chen SH, Wertz IE, Vucic D. Ubiquitination in the regulation
434   of inflammatory cell death and cancer. Cell Death Differ. 2021; 28: 591-605.

435   21.   Wang M, Han X, Yu T, Wang M, Luo W, Zou C, et al. OTUD1 promotes pathological cardiac
436   remodeling and heart failure by targeting STAT3 in cardiomyocytes. Theranostics. 2023; 13: 2263-
437   80.

438   22.   He B, Zhao YC, Gao LC, Ying XY, Xu LW, Su YY, et al. Ubiquitin-Specific Protease 4 Is an
439   Endogenous Negative Regulator of Pathological Cardiac Hypertrophy. Hypertension. 2016; 67:
440   1237-48.

441   23.   Wang B, Tang X, Yao L, Wang Y, Chen Z, Li M, et al. Disruption of USP9X in macrophages
442   promotes foam cell formation and atherosclerosis. J Clin Invest. 2022; 132(10).

443   24.   Withaar C, Meems LMG, Markousis-Mavrogenis G, Boogerd CJ, Silljé HHW, Schouten EM, et
444   al. The effects of liraglutide and dapagliflozin on cardiac function and structure in a multi-hit
445   mouse model of heart failure with preserved ejection fraction. Cardiovasc Res. 2021; 117: 2108-
446   24.

447   25.   Kon N, Kobayashi Y, Li M, Brooks CL, Ludwig T, Gu W. Inactivation of HAUSP in vivo modulates
448   p53 function. Oncogene. 2010; 29: 1270-9.

449   26.   Lange SM, Armstrong LA, Kulathu Y. Deubiquitinases: From mechanisms to their inhibition by
450   small molecules. Mol Cell. 2022; 82: 15-29.

451   27.   Jiang L, Xiong J, Zhan J, Yuan F, Tang M, Zhang C, et al. Ubiquitin-specific peptidase 7 (USP7)-
452   mediated deubiquitination of the histone deacetylase SIRT7 regulates gluconeogenesis. J Biol
453   Chem. 2017; 292: 13296-311.

454   28.   Pfeffer MA, Shah AM, Borlaug BA. Heart Failure With Preserved Ejection Fraction In
455   Perspective. Circ Res. 2019; 124: 1598-617.

456   29.   Lam CSP, Voors AA, de Boer RA, Solomon SD, van Veldhuisen DJ. Heart failure with preserved

457   ejection fraction: from mechanisms to therapies. Eur Heart J. 2018; 39: 2780-92.

458   30.   Roh J, Houstis N, Rosenzweig A. Why Don't We Have Proven Treatments for HFpEF? Circ Res.
459   2017; 120: 1243-5.

460   31.   Hu K, Ertl G. A new porcine model of hypertensive cardiomyopathy: a helpful tool to explore
461   the HFpEF mystique. Am J Physiol Heart Circ Physiol. 2015; 309: H1390-1.

462   32.   Dunlay SM, Roger VL, Redfield MM. Epidemiology of heart failure with preserved ejection
463   fraction. Nat Rev Cardiol. 2017; 14: 591-602.

464   33.   Pieske B, Tschöpe C, de Boer RA, Fraser AG, Anker SD, Donal E, et al. How to diagnose heart
465   failure with preserved ejection fraction: the HFA-PEFF diagnostic algorithm: a consensus
466   recommendation from the Heart Failure Association (HFA) of the European Society of Cardiology
467   (ESC). Eur Heart J. 2019; 40: 3297-317.

468   34.   Reddy YNV, Carter RE, Obokata M, Redfield MM, Borlaug BA. A Simple, Evidence-Based
469   Approach to Help Guide Diagnosis of Heart Failure With Preserved Ejection Fraction. Circulation.
470   2018; 138: 861-70.

471   35.   Valero-Muñoz M, Oh A, Faudoa E, Bretón-Romero R, El Adili F, Bujor A, et al. Endothelial-
472   Mesenchymal Transition in Heart Failure With a Preserved Ejection Fraction: Insights Into the
473   Cardiorenal Syndrome. Circ Heart Fail. 2021; 14: e008372.

474   36.   Zhang DH, Zhang JL, Huang Z, Wu LM, Wang ZM, Li YP, et al. Deubiquitinase Ubiquitin-
475   Specific Protease 10 Deficiency Regulates Sirt6 signaling and Exacerbates Cardiac Hypertrophy. J
476   Am Heart Assoc. 2020; 9: e017751.

477   37.   Ye B, Zhou H, Chen Y, Luo W, Lin W, Zhao Y, et al. USP25 Ameliorates Pathological Cardiac
478   Hypertrophy by Stabilizing SERCA2a in Cardiomyocytes. Circ Res. 2023; 132: 465-80.

479   38.   Dhingra R, Rabinovich-Nikitin I, Rothman S, Guberman M, Gang H, Margulets V, et al.
480   Proteasomal Degradation of TRAF2 Mediates Mitochondrial Dysfunction in Doxorubicin-
481   Cardiomyopathy. Circulation. 2022; 146: 934-54.

482   39.   Huang Z, Shen S, Wang M, Li W, Wu G, Huang W, et al. Mouse endothelial OTUD1 promotes
483   angiotensin II-induced vascular remodeling by deubiquitinating SMAD3. EMBO Rep. 2023; 24:
484   e56135.

485   40.   Pardali E, Sanchez-Duffhues G, Gomez-Puerto MC, Ten Dijke P. TGF-β-Induced Endothelial-
486   Mesenchymal Transition in Fibrotic Diseases. Int J Mol Sci. 2017; 18.

487   41.   Li J, Qu X, Yao J, Caruana G, Ricardo SD, Yamamoto Y, et al. Blockade of endothelial-
488   mesenchymal transition by a Smad3 inhibitor delays the early development of streptozotocin-
489   induced diabetic nephropathy. Diabetes. 2010; 59: 2612-24.

490   42.   Ju W, Ogawa A, Heyer J, Nierhof D, Yu L, Kucherlapati R, et al. Deletion of Smad2 in mouse
491   liver reveals novel functions in hepatocyte growth and differentiation. Mol Cell Biol. 2006; 26: 654-
492   67.

493   43.   Izzi L, Attisano L. Regulation of the TGFbeta signalling pathway by ubiquitin-mediated
494   degradation. Oncogene. 2004; 23: 2071-8.

495   44.   Herhaus L, Al-Salihi M, Macartney T, Weidlich S, Sapkota GP. OTUB1 enhances TGFβ
496   signalling by inhibiting the ubiquitylation and degradation of active SMAD2/3. Nat Commun. 2013;
497   4: 2519.

498   45.   Nan L, Jacko AM, Tan J, Wang D, Zhao J, Kass DJ, et al. Ubiquitin carboxyl-terminal hydrolase-
499   L5 promotes TGFβ-1 signaling by de-ubiquitinating and stabilizing Smad2/Smad3 in pulmonary
500   fibrosis. Sci Rep. 2016; 6: 33116.

501   46. Inui M, Manfrin A, Mamidi A, Martello G, Morsut L, Soligo S, et al. USP15 is a deubiquitylating
502   enzyme for receptor-activated SMADs. Nat Cell Biol. 2011; 13: 1368-75.
503   47. Huang YT, Cheng AC, Tang HC, Huang GC, Cai L, Lin TH, et al. USP7 facilitates SMAD3
504   autoregulation to repress cancer progression in p53-deficient lung cancer. Cell Death Dis. 2021;
505   12: 880.

506

507

Figure Legend

Figure 1 Endothelial USP7 expression was upregulated in HFpEF mice generated by a "Multiple-hit" strategy.

A, A schematic representation of the "Multiple-hit" strategy.

B, RNA transcriptome sequencing was used to reveal the expression profile of DUBs (deubiquitinating enzymes) in HFpEF mice. RNA transcriptome sequencing was performed on control (n = 4) and HFpEF (n = 4) mice heart samples, respectively. We use log2 of the fold change as the source of data for the x axis and −log10 of the P as the source of data for the y axis. Fold change > 1.5× and P < 0.05 indicate statistically significant differences. Red and green points represent the upregulated DUBs and the downregulated DUBs compared with control group. Red arrow labeled represents the exact point of USP7; Although, black points represent the DUBs with no statistical difference compared with the control group.

C, Representative western blotting for USP7 in normal heart tissue and HFpEF heart tissue in HFpEF mice and densitometric quantification of USP7, n = 6.

D, Real-time qPCR analysis of the mRNA expression of USP7 in primary cardiomyocytes, primary ECs, cardiac fibroblast and macrophages isolated from HFpEF mice heart tissue.

E, Representative western blot analysis for USP7 protein levels in primary cardiomyocytes, ECs, cardiac fibroblast and macrophages. GAPDH was used as loading control.

F, Immunofluorescence staining and quantification of USP7 (red) and CD31 (green) in the isolated primary ECs from HFpEF mice. Scale bars, 20 μm.

G, Immunofluorescence staining of USP7(red) and CD31(green) on cross sections of the heart tissues from mice under "Multiple-hit" strategy insult and mice under normal diet. Scale bars, 20 μm.

C-F: Student t test; number of comparisons = 12(**C**), number of comparisons = 8(**D-F**); DAPI indicates 4'6-diamidino-2-phenylindole; HFD, high-fat diet; ECs, endothelial cells; HFpEF, heart failure with preserved ejection fraction; The protein level was standardized by GAPDH from each group was normalized to 1 value from the control group, which was set to 1.

Figure 2 EC-specific knockout of USP7 alleviates cardiac fibrosis by mitigating EndMT, thereby ameliorating the HFpEF phenotypes.

USP7^flox/flox^ and USP7-ECKO mice were subjected to normal diet and "Multiple-hit" strategy.

A, Representative whole heart image from mice in each group.

B and **C**, Masson (**B**) and Sirius Red (**C**) in sections of hearts. (Scale bar, 1 mm and 100 μm for Masson; 100 μm for Sirius Red staining).

D and **E**, Quantification of fibrosis by assessing the Masson(**O**) and SR-positive(**P**) areas, n = 4.

F, Heart weight (HW) normalized to tibia length (TL).

G, Ratio between wet and dry lung weight.

H, Percentage of left ventricular ejection fraction (LVEF).

I, Ratio between mitral E wave and E′ wave (E/E′).

J, Percentage of global longitudinal strain (GLS).

K, The serum levels of BNP (B-type natriuretic peptide) in four groups.

549   **L**, Representative immunofluorescent staining images and quantification of microvascular

550   endothelial cell CD31 (green) and fibrosis marker α-SMA (red) in the heart tissues (n = 4). Scale

551   bar, 20 μm.

552   **M**, Representative western blot analysis for endothelial cell marker (VE-cadherin), mesenchymal

553   marker (α-SMA, Vimentin) from the heart tissues of four groups.

554   **N**, Real-time qPCR analysis of endothelial cell marker (*Cdh5*), mesenchymal marker (*Acta2, Vim*)

555   and transcription factors of EndMT (*Twist1, Snail1*) in heart tissues. n = 4.

556   **D-L, N**: 1-way ANOVA followed by Tukey post-hoc tests; Data are shown as mean±SEM and

557   adjusted P values were provided in case of multiple groups. The protein level was standardized by

558   GAPDH and the mRNA level from each group was normalized to 1 value from the control group,

559   which was set to 1.

560

561   **Figure 3 USP7 is involved in endothelial EndMT in vitro.**

562   **A** and **B**, Representative western blotting analysis (**A**) and densitometric quantification (**B**) of

563   USP7 under different TGFβ1 stimulation in primary cardiac microvascular endothelial cells

564   (CMECs). n =4.

565   **C** and **D**, Representative western blotting analysis (**C**) and densitometric quantification (**D**) of

566   USP7 under different treating time of TGFβ1 stimulation(10ng/ml) in primary cardiac

567   microvascular endothelial cells (CMECs). n = 4.

568   **E** and **F**, Representative western blotting analysis (**E**) and densitometric quantification (**F**) of

569   endothelial cell marker (CD31, VE-cadherin), mesenchymal marker (α-SMA, Vimentin) and

570   transcription factors of EndMT (Twist1) in primary cardiac microvascular endothelial cells

571   (CMECs) transfected with short hairpin RNA lentiviral particles targeting USP7 (shUSP7) or

572   control adenovirus (sh-Vector) under TGFβ1 stimulation (10ng/ml, 72h) or PBS control. n = 4.

573   **G**, Expression analysis by RT-qPCR of endothelial marker (Cdh5 and Pecam1), mesenchymal

574   marker (Acta2 and Vim) and transcription factors of EndMT (Twist1 and Snail1) in primary

575   cardiac microvascular endothelial cells (CMECs) transfected with short hairpin RNA lentiviral

576   particles targeting USP7 (shUSP7) or control adenovirus (sh-Vector) under TGFβ1 stimulation

577   (10ng/ml, 72h) or PBS control. n = 4.

578   **H** and **I**, Immunofluorescence staining of CD31 (green) and α-SMA (red) (**H**) and bright field

579   image (**I**) in transfected CMECs (sh-Vector or sh-USP7) were either untreated or treated with

580   TGFβ1 for 72 hours. Scale bars, 20 μm(**H**), 200 μm(**I**).

581   **J** and **K**, Quantification of EndMT of CMECs by assessing the α-SMA intensity(**J**) of **H** and

582   percentage of spindle-shaped cells(**K**) in **I**, n = 4.

583   **B, D:** 2-way ANOVA followed by Dunnett's multiple comparisons tests; **F, G, J, K:** 1-way

584   ANOVA followed by Tukey post-hoc tests; Data are shown as mean±SEM and adjusted P values

585   were provided in case of multiple groups. The protein level was standardized by GAPDH, the

586   mRNA level and α-SMA intensity from each group was normalized to 1 value from the control

587   group, which was set to 1.

588

589   **Figure 4 USP7 directly interacts with SMAD3.**

590   **A**, Schematic illustration of quantitative proteomic screen.

591   **B**, Coomassie Blue staining of potential target proteins of USP7.

C and D, CMECs were transfected with short hairpin RNA lentiviral particles targeting USP7 (shUSP7) for 24 h, while the control cells were transfected with control adenovirus (sh-Vector), Levels of USP7 and SMAD3 protein were measured by western blotting analysis (**C**) and densitometric quantification (**D**), n = 6.

E and **F**, CMECs were transfected with SMAD3 siRNA for 24 h, while the control cells were transfected with negative control (NC) siRNA. Levels of SMAD3 and USP7 protein were measured by western blotting analysis (**E**) and densitometric quantification (**F**), n = 6.

G and **H**, Coimmunoprecipitation of USP7 and SMAD3 in CMECs treated with or without TGFβ1 stimulation. Endogenous USP7 was immunoprecipitated by anti-USP7 antibody (**G**) and Endogenous SMAD3 was immunoprecipitated by anti-SMAD3 antibody (**H**). IgG, immunoglobulin G. n = 3.

I and **J**, Coimmunoprecipitation of USP7 and SMAD3 in 293T cells co-transfected with Flag-USP7 and Myc-SMAD3 plasmids. Exogenous USP7 was immunoprecipitated by anti-Flag antibody(**I**) and exogenous SMAD3 was immunoprecipitated by anti-Myc antibody(**J**), n = 3.

K, Schematic illustration of the USP7 domain deletion construct used in **L**.

L, Coimmunoprecipitation of WT-USP7, Mut-USP7, and SMAD3 in 293T cells co-transfected with overexpression plasmids of Flag-WT-USP7, Flag-Mut-USP7 and Myc-SMAD3. Exogenous normal or mutated USP7 was immunoprecipitated by anti-Flag antibody. n = 3.

D, **F**: Student t test; number of comparisons = 6; The protein level was standardized by GAPDH from each group was normalized to 1 value from the sh-Vector/si-NC group, which was set to 1.

Figure 5 USP7 regulates the stability of SMAD3 protein through deubiquitination.

A and **B**, Representative western blotting (**A**) and real-time qPCR (**B**) for USP7 and SMAD3 in CMECs transfected with short hairpin RNA lentiviral particles targeting USP7 (shUSP7) or control adenovirus (sh-Vector), and treated for MG132 or PBS for 4 hours. n = 6.

C and D, Representative western blotting for USP7 and SMAD3 in CMECs co-transfected with control adenovirus or recombinant USP7 adenovirus and then subjected to CHX pulse-chase assay (**C**) and densitometric quantification of SMAD3 (**D**). n = 4.

E, Western blot analysis of indicated proteins in 293T cells cotransfected with Myc-SMAD3 and HA-Ub in the presence of Flag-vector or Flag-USP7 plus the proteasome inhibitor MG132 (10 μM) for 4 hours before IP of whole cell lysates with MYC magnetic beads (n = 3).

F, Coimmunoprecipitation of USP7 and SMAD3 in 293T cells co-transfected with Flag-USP7 or Flag-USP7-C223S and Myc-SMAD3 plasmids. Exogenous SMAD3 was immunoprecipitated by anti-Myc antibody, n = 3.

G, Western blot analysis of indicated proteins in 293T cells cotransfected with Myc-SMAD3 and HA-Ub in the presence of Flag-vector, Flag-USP7 or Flag-USP7-C223S plus the proteasome inhibitor MG132 (10 μM) for 4 hours before IP of whole cell lysates with MYC magnetic beads (n = 3).

H, Western blot analysis of indicated proteins in 293T cells cotransfected with Myc-SMAD3 and HA-Ub, HA-K48 and HA-K63 in the presence of Flag-vector or Flag-USP7 plus the proteasome inhibitor MG132 (10 μM) for 4 hours before IP of whole cell lysates with MYC magnetic beads (n = 3).

B: 1-way ANOVA followed by Tukey post-hoc tests; **D**, 2-way ANOVA plus Šídák's multiple comparisons test; Data are shown as mean±SEM and adjusted P values were provided in case of

multiple groups. The protein level was standardized by GAPDH or β-actin and the mRNA level
from each group was normalized to 1 value from the control group, which was set to 1.

Figure 6 USP7 Regulates EndMT by stabilizing SMAD3 and accumulating phosphorylated SMAD3

A, Representative western blotting analysis and densitometric quantification of endothelial cell marker (CD31, VE-cadherin), and mesenchymal marker (α-SMA, Vimentin) in primary cardiac microvascular endothelial cells (CMECs) cotransfected with short hairpin RNA lentiviral particles targeting USP7 (shUSP7)/control adenovirus (sh-Vector) and control adenovirus (Ad-Vector)/recombinant SMAD3 adenovirus (Ad-SMAD3) under TGFβ1 stimulation (10 ng/ml, 72h) or PBS control. n = 4.

B, Representative western blotting analysis (**C**) and densitometric quantification (**D**) of p-SMAD3 and SMAD3 protein level in primary cardiac microvascular endothelial cells (CMECs) transfected with short hairpin RNA lentiviral particles targeting USP7 (shUSP7)/control adenovirus (sh-Vector) under TGFβ1 stimulation (10 ng/ml, 72h) or PBS control. n = 4.

C, Representative western blotting analysis of p-SMAD3 and SMAD3 protein level in cytoplasm and nucleus in primary cardiac microvascular endothelial cells (CMECs). β-Tubulin was used as the loading control for cytosolic fractions. Histone 3 was used as the loading control for nuclear fractions. n = 4.

D, Immunofluorescence staining of SMAD3 (red) and DAPI (blue) in primary cardiac microvascular endothelial cells (CMECs) transfected with short hairpin RNA lentiviral particles targeting USP7 (shUSP7)/control adenovirus (sh-Vector) under TGFβ1 stimulation (10 ng/ml, 72h) or PBS control. Scale bars, 20 μm.

A, B: 1-way ANOVA followed by Tukey post-hoc tests; Data are shown as mean±SEM and adjusted P values were provided in case of multiple groups. The protein level was standardized by GAPDH from each group was normalized to 1 value from the control group, which was set to 1.

Figure 7 USP7 ameliorates cardiac fibrosis and EndMT of HFpEF by stabilizing SMAD3 in vivo.

A, Schematic of the experimental setup. After "Multiple-hit" strategy for 12 weeks, recombinant AAV9-ENT vectors carrying SMAD3 or ctrl were injected to heart of mice in situ for 2 weeks.

B, Heart weight (HW) normalized to tibia length (TL).

C, Ratio between wet and dry lung weight.

D, Percentage of left ventricular ejection fraction (LVEF).

E, Ratio between mitral E wave and E′ wave (E/E′).

F, Percentage of global longitudinal strain (GLS).

G, The serum levels of NT-proBNP (N-terminal pro-B-type natriuretic peptide).

H and **I**, Representative and quantification in Masson (**B**) and Sirius Red (**C**) staining in sections of hearts. (Scale bar, 100 μm for Masson; 100 μm for Sirius Red staining).

J, Representative immunofluorescent staining images and quantification of microvascular endothelial cell CD31 (green) and fibrosis marker α-SMA (red) in the heart tissues (n = 4). Scale bar, 20 μm.

B-J: 1-way ANOVA followed by Tukey post-hoc tests; Data are shown as mean±SEM and adjusted P values were provided in case of multiple groups.

680

Figure 8 A schematic diagram of this study.

In normal endothelial cells, SMAD3 undergoes ubiquitination and normal degradation. However, under various metabolic-hit conditions, the abnormal increasing USP7 leads to a reduction in SMAD3 ubiquitination and degradation. This, in turn, promotes the activation of SMAD3, facilitating its entry into the nucleus and promoting the EndMT process. Consequently, this cascade of events contributes to cardiac fibrosis and HFpEF. Ub, ubiquitin; EndMT. endothelial-to-mesenchymal transition; HFpEF, heart failure with preserved ejection fraction.

688

689 **Non-standard Abbreviations and Acronyms**

Ang II	angiotensin II
ARNI	angiotensin receptor–neprilysin inhibitor
BNP	B-type natriuretic peptide
CHX	cycloheximide
CMECs	cardiac microvascular endothelial cells
Co-IP	co-immunoprecipitation
DUBs	deubiquitinating enzymes
ECM	extracellular matrix
ECs	endothelial cells
EMT	epithelial-mesenchymal transition
EndMT	endothelial-mesenchymal transition
GLS	global longitudinal strain
HF	heart failure
HFpEF	heart failure with preserved ejection fraction
HFrEF	heart failure with reduced ejection fraction
HW/TL	heart weight-to-tibia length ratio
IVRT	isovolumic relaxation time
LVEF	left ventricular ejection fraction
LVPWd	left ventricular posterior wall thickness in diastole
MI	myocardial infarction
NO	nitric oxide
PAH	pulmonary arterial hypertension
p-SMAD3	phosphorylated SMAD3
SGLT2i	sodium–glucose cotransporter 2 inhibitor
USP7	ubiquitin-specific protease 7

690